Diffusion Parameters and Growth Mechanism of Phases in the Cu-Sn System

A. PAUL, C. GHOSH, and W.J. BOETTINGER

The tracer diffusion coefficients of the elements as well as the integrated interdiffusion coefficients are determined for the Cu_3Sn and Cu_6Sn_5 intermetallic compounds using incremental diffusion couples and Kirkendall marker shift measurements. The activation energies are determined for the former between 498 K and 623 K (225 °C and 350 °C) and for the latter between 423 K and 473 K (150 °C and 200 °C). Sn is found to be a slightly faster diffuser in Cu_6Sn_5, and Cu is found to be the faster diffuser in Cu_3Sn. The results from the incremental couples are used to predict the behavior of a Cu/Sn couple where simultaneous growth of both intermetallics occurs. The waviness at the Cu_3Sn/Cu_6Sn_5 interface and possible reasons for not finding Kirkendall markers in both intermetallics in the Cu/Sn couple are discussed.

I. INTRODUCTION

THE reaction between Sn-based solders and Cu-based metallization remains an important topic. Increased miniaturization and conversion to Pb-free solders place increasing demands on the electromechanical integrity of solder joints, whether they be chip to chip, chip to substrate, or package level. Because of interdiffusion, two intermetallic compounds, Cu_3Sn and Cu_6Sn_5, usually form during soldering and or pretinning of Cu substrates and can continue to grow during storage or service. Because these intermetallics affect the integrity of joints, many articles have been published on this topic (e.g., References 1 and 2).

The diffusion literature in Sn-Cu alloys was reviewed in 1981 by Butryrmowicz.[3] In Cu solid solutions, Sn is the fast diffuser.[4,5] On the other hand, Cu is known to be an extremely fast interstitial diffuser in the c direction in Sn.[6] However, in the present research, we focus on diffusion in the intermetallic compounds. This subject was studied using diffusion couples by Onishi and Fujibuchi.[7] They obtained parabolic growth constants for the layer thicknesses, measured the range of stoichiometry of the phases, and determined values for the interdiffusion coefficients for the Cu_3Sn and Cu_6Sn_5 phases between 463 K and 493 K (190 °C and 220 °C), as follows:

$$\tilde{D}_{Cu_6Sn_5} = 1.55 \times 10^{-8} \exp\left(-64.8\,kJ\,mol^{-1}/RT\right)\,m^2/s$$

$$\tilde{D}_{Cu_3Sn} = 1.43 \times 10^{-8} \exp\left(-70.7\,kJ\,mol^{-1}/RT\right)\,m^2/s$$

Further, in their Cu/Sn couples, Kirkendall markers were observed only in the Cu_6Sn_5 phase. Thus, they observed marker motion toward the Sn-rich side of the Matano interface and concluded that Sn was the faster diffuser in Cu_6Sn_5. A detailed analysis of the mobilities of species was not possible in their work, because the marker movement was less than their diameter (5 μm). In the present study, 1-μm markers were employed. We also employ integrated diffusion coefficients, as introduced by Wagner,[8] due to the uncertainty of the exact composition range of an intermetallic compound as measured from a diffusion couple with a microprobe.

Tu and Thompson[9] interestingly found that only Cu_6Sn_5 grew, and not Cu_3Sn, at room temperature in thin film Cu/Sn bilayers. Cu_3Sn could grow only above 423 K (150 °C). Their W markers after room temperature diffusion were found in the Cu_6Sn_5 phase much closer to the Cu/Cu_6Sn_5 interface than to the Cu_6Sn_5/Sn interface. Thus, both Sn and Cu diffuse in Cu_6Sn_5, and the authors concluded that Cu was the faster diffuser in Cu_6Sn_5. Paul et al.[10] prepared incremental diffusion couples of Cu/Cu_6Sn_5 and Cu_3Sn/Sn with Kirkendall markers to measure separately the diffusion properties in the intermetallics Cu_3Sn and Cu_6Sn_5, respectively. They determined the ratio of tracer diffusivities at a single temperature, 488 K (215 °C), for Cu_3Sn as $D_{Cu}^*/D_{Sn}^* \approx 1.1$ and for Cu_6Sn_5 as $D_{Cu}^*/D_{Sn}^* \approx 0.65$. The latter ratio indicates that in Cu_6Sn_5, Cu is a slower diffuser than Sn contrary to the conclusion of Reference 9. Due to the discrepancy of these results, additional work on this system is warranted. Furthermore, there is no knowledge of the individual tracer diffusivities or their activation energies in the intermetallics.

Bulk single-phase intermetallic specimens prepared by Schaefer et al.[11] are used in the present study to make incremental diffusion couples. We report the results and employ analysis to determine the integrated interdiffusion coefficient and tracer diffusion coefficients of the

A. PAUL, Associate Professor, and C. GHOSH, PhD Student, are with the Department of Materials Engineering, Indian Institute of Science, Bangalore, India. W.J. BOETTINGER, NIST Fellow, is with the Metallurgy Division, NIST, Gaithersburg, MD 20899. Contact e-mail: william.boettinger@nist.gov

elements over a range of temperatures for both Cu_3Sn and Cu_6Sn_5. The behavior of a Cu/Sn couple will then be predicted from the data obtained from the incremental couples and compared to experiment.

The relative rates of diffusion of Cu and Sn are relevant in two areas of electronic packaging. It is important to determine whether porosity observed in solder joints is due to the Kirkendall effect or other sources such as incorporated organic material from electroplating. Also intermetallic growth in solder joints is widely thought to generate compressive stress that causes Sn whisker growth. The mechanism of stress generation has been recently ascribed to the volume change of intermetallic, its nonplanar interface morphology, and the relative rates of diffusion.[12,13]

II. EXPERIMENTAL PROCEDURE

A Cu/Sn diffusion couple and incremental diffusion couples, Cu/Cu_6Sn_5 and Cu_3Sn/Sn, were examined. The latter two enable the individual growth of Cu_3Sn and Cu_6Sn_5 phases, respectively. This permits the measurement of marker shifts in each intermetallic. Cu with a purity of 0.9999 mass fraction and Sn with a purity of 0.99999 mass fraction were used in this study. Bulk single-phase Cu_3Sn and Cu_6Sn_5 intermetallic compound samples were made by liquid atomization, rapid solidification, and hot isostatic pressing (HIP) of alloys of composition Cu_3Sn and Cu_6Sn_5.[11] This procedure was employed because of the difficulty of obtaining samples of single-phase intermetallic compound. Because both Cu_6Sn_5 and Cu_3Sn form by peritectic reactions, the ordinary casting of samples with the composition of the intermetallics yields a three-phase structure that could not be annealed into single-phase material. The rapid freezing of atomization produces a sufficiently fine structure that HIP produced annealed, 100 pct dense single-phase materials. Indeed some of this material was used to measure physical, mechanical, and wetting properties of the bulk intermetallics.[14,15] To prepare diffusion couples, the samples were cut to 1-mm thickness and 7 mm × 7 mm cross section, prepared by standard metallographic grinding down to 2000-grit paper and further polished using 1-μm diamond paste. To serve as Kirkendall markers, TiO_2 inert particles of approximately 1-μm size were dispersed (approximately 2 to 3 particles/100 μm^2) at the bonding interface before clamping prior to diffusion anneals. Samples were then sealed in quartz capsules in vacuum (approximately 10^{-4} Pa) and annealed for various times at different temperatures. The diffusion couples were sliced with a slow speed saw, prepared by standard metallographic grinding and polishing. Examination was performed in a scanning electron microscope. Energy dispersive X-ray analysis was used after taking standards from pure elements to measure the composition profile and to determine the position of TiO_2 particles. A low density of markers was used so as to not disrupt the interdiffusion process. However, this leads to a scarcity of observed marker particles in any given cross section.

Marker positions were always determined from an average of several particles.

III. RESULTS

A. Cu/Sn Couple

A scanning electron micrograph of the Cu/Sn diffusion couple annealed at 473 K (200 °C) for 225 hours is shown in Figure 1. As expected from the phase diagram, two intermetallic compounds, Cu_3Sn and Cu_6Sn_5, grow in the interdiffusion zone. The position of the Kirkendall marker plane was detected from the location of the TiO_2 particles in the Cu_6Sn_5 phase. We note the nonplanar nature of the interfaces bounding the Cu_6Sn_5 phase, which we discuss in Section IV.

The phases grow with very narrow composition range in accord with the phase diagram. Thus, it is difficult to accurately measure the small concentration gradient across the phase to determine the interdiffusion coefficient by conventional methods. To circumvent this problem, Wagner[8] introduced the concept of an integrated interdiffusion coefficient, $\tilde{D}_{int}$ (m^2/s), for a binary alloy defined for a phase β, for example, by

$$\tilde{D}_{int}^\beta = \int_{N_i'}^{N_i''} \tilde{D}^\beta dN_i \qquad [1]$$

where $\tilde{D}^\beta$ (m^2/s) is the unknown and possibly composition-dependent β-phase interdiffusion coefficient, N_i is the mol fraction of component i, and N_i' and N_i'' are the unknown limits of homogeneity range of the phase. For a diffusion couple, which (a) has end members that are pure elements with negligible solubility or intermetallics with negligible solubility range and (b) forms only intermetallic phases with narrow homogeneity range, Wagner has shown that the integrated interdiffusion coefficient of each phase that forms can be calculated using the expression
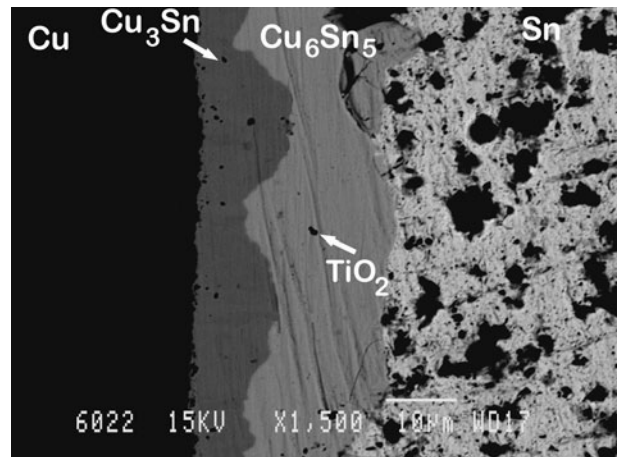

Fig. 1—Interdiffusion zone in the Cu/Sn system annealed at 473 K (200 °C) for 225 h is shown. TiO_2 particles used as inert markers were found in the Cu_6Sn_5 phase.

$$\tilde{D}_{\text{int}}^{\beta} = \frac{\left(N_i^{\beta} - N_i^{-}\right)\left(N_i^{+} - N_i^{\beta}\right)}{\left(N_i^{+} - N_i^{-}\right)} \frac{\Delta x_{\beta}^2}{2t}$$
$$+ \left[\left(\frac{N_i^{+} - N_i^{\beta}}{N_i^{+} - N_i^{-}} \right) \sum_{v=2}^{v=\beta-1} \left(\frac{V_m^{\beta}}{V_m^{v}} (N_i^{v} - N_i^{-}) \Delta x_v \right) \right.$$
$$\left. + \left(\frac{N_i^{\beta} - N_i^{-}}{N_i^{+} - N_i^{-}} \right) \sum_{v=\beta+1}^{v=n-1} \left(\frac{V_m^{\beta}}{V_m^{v}} (N_i^{+} - N_i^{v}) \Delta x_v \right) \right] \frac{\Delta x_{\beta}}{2t}$$

[2]

where (a) β is the phase of interest; (b) $N_i^{\pm}$ is the mole fraction of element i, with "–" and "+" indicating the left- and right-hand-side end members, respectively; (c) V_m^v and Δx_v are the molar volume and layer thickness of the vth phase; and (d) t is the annealing time. We note that the two summations cover the phases to the left and right of the phase of interest, respectively. The composition of the phases are taken as $N_{\text{Sn}}^{+} = 0$, $N_{\text{Sn}}^{\text{Cu}_3\text{Sn}} = 1/4$, $N_{\text{Sn}}^{\text{Cu}_6\text{Sn}_5} = 5/11$, and $N_{\text{Sn}}^{-} = 1$. The molar volume of the product phases for the present case are calculated as $V_m^{\text{Cu}_3\text{Sn}} = 8.59$ and $V_m^{\text{Cu}_6\text{Sn}_5} = 10.59\,\text{cm}^3/\text{mol}$ (4.4 atoms in a unit cell; Section IV–A) from the lattice parameter data available in the literature.[16] For $t = 225$ hours at 473 K (200 °C), the measured average layer thicknesses of the phases were found to be $\Delta x_{\text{Cu}_3\text{Sn}} = 9\,\mu\text{m} \pm 3.6\,\mu\text{m}$ and $\Delta x_{\text{Cu}_6\text{Sn}_5} = 16.4\,\mu\text{m} \pm 2.1\,\mu\text{m}$, giving parabolic growth constants defined by

$$k_p = \frac{(\Delta x_i)^2}{2t}$$

[3]

of $5 \times 10^{-17}\,\text{m}^2/\text{s}$ and $1.6 \times 10^{-16}\,\text{m}^2/\text{s}$ for Cu_3Sn and Cu_6Sn_5, respectively. The integrated diffusion coefficients determined from Eq. [2] are $\tilde{D}_{\text{int}}^{\text{Cu}_3\text{Sn}} = 1.94 \times 10^{-17}\,\text{m}^2/\text{s}$ and $\tilde{D}_{\text{int}}^{\text{Cu}_6\text{Sn}_5} = 5.64$. Onishi and Fujibuchi[7] obtained parabolic growth constants of $3.84 \times 10^{-17}\,\text{m}^2/\text{s}$ and $1.12 \times 10^{-16}\,\text{m}^2/\text{s}$ at 473 K (200 °C) for Cu_3Sn and Cu_6Sn_5, respectively, in general agreement with our values. Using their measured stoichiometric widths of the Cu_3Sn and Cu_6Sn_5 phases at 473 K (200 °C) of 0.013 and 0.015 atomic fraction, respectively, and their interdiffusion coefficients, we can estimate integrated diffusivities from their experiments directly from Eq. [1] of $8 \times 10^{-18}\,\text{m}^2/\text{s}$ and $1.5 \times 10^{-17}\,\text{m}^2/\text{s}$, which generally agree with our numbers but are a factor of 2 to 3 smaller.

In addition to the interdiffusion data, the ratio of intrinsic diffusivities in an A-B binary system can be determined from our experiments at the location and in the phase where the Kirkendall marker plane is found. Following analysis by van Loo,[17] the ratio at the marker position only is given by

$$\frac{D_B}{D_A} = \frac{\bar{V}_B}{\bar{V}_A} \left[\frac{N_B^{+} \int_{-\infty}^{x_K} \frac{Y}{V_m} dx - N_B^{-} \int_{x_K}^{+\infty} \frac{(1-Y)}{V_m} dx}{-N_A^{+} \int_{-\infty}^{x_K} \frac{Y}{V_m} dx + N_A^{-} \int_{x_K}^{+\infty} \frac{(1-Y)}{V_m} dx} \right]$$

[4]

where D_i and $\bar{V}_i$ are the intrinsic diffusion coefficients and partial molar volumes of element i in the phase of

interest, $Y = \left(N_B - N_B^{-}\right)/\left(N_B^{+} - N_B^{-}\right)$ is the Sauer–Freise scaled mole fraction variable,[18] and x_K is the location of the marker plane. While this expression is often proven in the literature only for single-phase diffusion couples, it is also correct when applied to multiphase diffusion couples consisting of planar layers; *i.e.*, when the diffusion can be described by the similarity variable $xt^{-1/2}$. The conservation of A and B components at interfaces allows one to merely integrate through the jumps in composition at the interphase interfaces. For the same reason, the Sauer–Freise expression for the interdiffusion coefficient also apples to multiphase diffusion couples.

However, a difficulty remains with the determination of the partial molar volumes for a phase with very narrow homogeneity range. One often assumes that the partial molar volumes of species A and B are equal. However, V_m in a phase may change very sharply within the narrow composition range, and this assumption can lead to a huge error in the calculation of intrinsic diffusivities of the elements. On the other hand, one does not need the partial molar volumes if we seek only information about the ratio of tracer diffusivities of the elements, which is given by

$$\frac{D_A^*}{D_A^*} = \frac{V_B D_A (1 - W_B)}{V_A D_B (1 + W_A)}$$

[5]

where the W_i terms are the vacancy wind factors.[19] For substitutional diffusion, the vacancy wind factors are known to be quite small. In nonstoichiometric B2 intermetallic phases, these factors were shown to be quite important when diffusion occurs by a six-jump cycle diffusion mechanism.[20] Due to the complex crystal structures of the intermetallics in the current article and the lack of knowledge about their diffusion mechanisms, we will neglect the wind factors in the present work, especially as this is the first extensive report of intrinsic diffusion in this system. Thus, we will use the approximation that

$$\frac{D_B^*}{D_A^*} = \left[\frac{N_B^{+} \int_{-\infty}^{x_K} \frac{Y}{V_m} dx - N_B^{-} \int_{x_K}^{+\infty} \frac{(1-Y)}{V_m} dx}{-N_A^{+} \int_{-\infty}^{x_K} \frac{Y}{V_m} dx + N_A^{-} \int_{x_K}^{+\infty} \frac{(1-Y)}{V_m} dx} \right]$$

[6]

With the measured average marker distance of 7 μm from the location of the $\text{Cu}_3\text{Sn}/\text{Cu}_6\text{Sn}_5$ interface, the ratio $D_{\text{Cu}}^*/D_{\text{Sn}}^* = 0.77$ in the Cu_6Sn_5 phase. This compares to $D_{\text{Cu}}^*/D_{\text{Sn}}^* = 0.65$ for Cu_6Sn_5 obtained by Reference 10 at 488 K (215 °C), as described previously.

It should be noted that, while we are able to determine the ratio of D^* of elements in Cu_6Sn_5 phase, we are not able to determine the ratio in the Cu_3Sn phase from this experiment, because no Kirkendall markers where found in the Cu_3Sn phase. To determine the ratio of D^*'s in the Cu_3Sn phase and to confirm that obtained in Cu_6Sn_5, we need to conduct interdiffusion studies with incremental diffusion couples, so that only one phase grows in the interdiffusion zone.

B. Incremental Couples Cu/Cu₆Sn₅ and Cu₃Sn/Sn

1. Parabolic growth constants

To grow Cu₃Sn, incremental diffusion couples Cu/Cu₆Sn₅ were annealed between 498 K and 623 K (225 °C and 350 °C) for 225 hours. Below this temperature range, bonding of the end members failed. To grow Cu₆Sn₅, incremental diffusion couples Cu₃Sn/Sn were annealed between 423 K and 473 K (150 °C and 200 °C) for 225 hours (Table I). The upper temperature was set by the Sn melting point. Examples of the interdiffusion zones grown in these two incremental couples are shown in Figures 2(a) through (c). The average widths of the intermetallics and the positions of the marker plane, as evident from the location of TiO₂ particles, were measured. Moreover, in the Cu₃Sn phase, the position of the marker plane can easily be detected from the duplex morphology present in the interdiffusion zone demarcated by the white line in Figure 2(b). We note the nonplanar nature of the interfaces bounding the Cu₆Sn₅ phase in Figure 2(c). Parabolic growth constants for Cu₃Sn and Cu₆Sn₅ at each temperature are plotted in Figures 3(a) and (b), respectively, following the Arrhenius equation:

$$k_P = k_p^0 \exp\left(-\frac{Q}{RT}\right) \qquad [7]$$

where k_p^0 is the pre-exponential factor, Q (J/mol) is the activation energy, T is the temperature in K, and R ($= 8.314$ J/mol·K) is the gas constant. The values for the pre-exponentials and the activation energies are given on the graphs. We note that because of the waviness of the layers, the measured thicknesses of layers as well as the distances between interfaces and markers are considered to be accurate to approximately 30 pct, a figure that leads to an uncertainty in the derived parabolic growth constants and diffusion coefficients in Figures 3(a) and 3(b), 4(a) and 4(b), and 6(a) and 6(b) of approximately 60 pct.

2. Integrated interdiffusion coefficients

The values of $\tilde{D}_{int}$ of the phases were calculated following Eq. [1] and plotted as a function of $1/T$ based on the Arrhenius equation:

$$\tilde{D}_{int} = \tilde{D}_{int}^0 \exp\left(-\frac{Q}{RT}\right) \qquad [8]$$

where $\tilde{D}_{int}^0$ (m²/s) is the pre-exponential factor. The results for Cu₃Sn and Cu₆Sn₅ are shown in Figures 4(a) and (b), respectively, and are given in Table I along with other information to be described subsequently. The $\tilde{D}_{int}$ values for both intermetallics obtained from the Cu/Sn diffusion couple at 473 K (200 °C) (Section III−A) are also shown in the graphs (squares). We note agreement between the data points from the Sn/Cu couple and the data from the incremental couples. The activation energies are found to be $Q_{Cu_3Sn} = 73.8$ kJ/mol and $Q_{Cu_6Sn_5} = 81$ kJ/mol. The activation energy for the integrated diffusion coefficient of the phases is found to be similar to the data determined by Onishi and Fujibuchi.[7]

3. Tracer diffusion coefficients

We now determine the ratio of the tracer diffusivities of elements in each intermetallic phase from the marker positions determined in the incremental couples. Then, using thermodynamic data for the Sn-Cu system, we extract the individual tracer coefficients.

From the incremental couples, measurement of the location of the markers within the intermetallic phase permits the estimation of the ratio of D^*'s at the position of the marker planes using Eq. [6] for both Cu₃Sn and Cu₆Sn₅. The calculated ratios at the different temperatures are listed in Table I. We find that the average value for Cu₃Sn is $D_{Cu}^*/D_{Sn}^* \approx 30$ and and that for Cu₆Sn₅ is $D_{Cu}^*/D_{Sn}^* \approx 0.35$. Thus, Cu is faster in Cu₃Sn and Sn is faster in Cu₆Sn₅ over the temperature ranges studied.
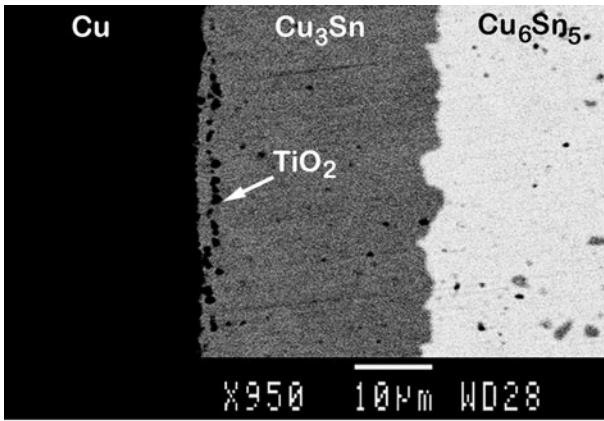
To extract individual tracer diffusivities, not just the ratios, we follow the method proposed in Reference 21. The interdiffusion coefficient $\tilde{D}^{Cu_3Sn}$ for the Cu₃Sn phase (for example) is related to tracer diffusivities D_{Cu}^* and D_{Sn}^*:

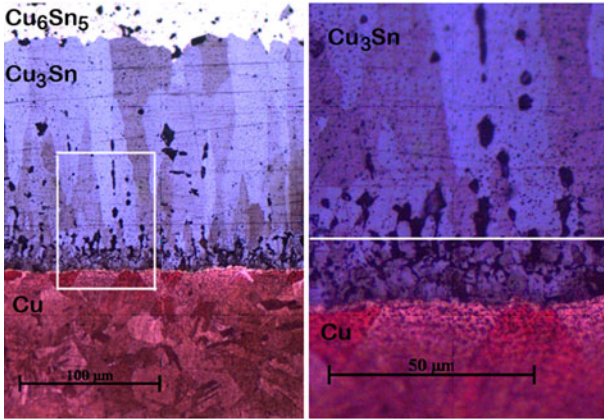$$\tilde{D}^{Cu_3Sn} = \left(N_{Cu}^{Cu_3Sn} D_{Sn}^* + N_{Sn}^{Cu_3Sn} D_{Cu}^*\right) W_{AB} \left(\frac{d\ln a_{Sn}}{d\ln N_{Sn}}\right) \qquad [9]$$

where $\frac{d\ln a_{Sn}}{d\ln N_{Sn}} = \frac{d\ln a_{Cu}}{d\ln N_{Cu}}$ is the thermodynamic parameter; a_{Cu} and a_{Sn} are the activities of the elements in Cu₃Sn; and W_{AB} is Manning's vacancy wind parameter,[19]
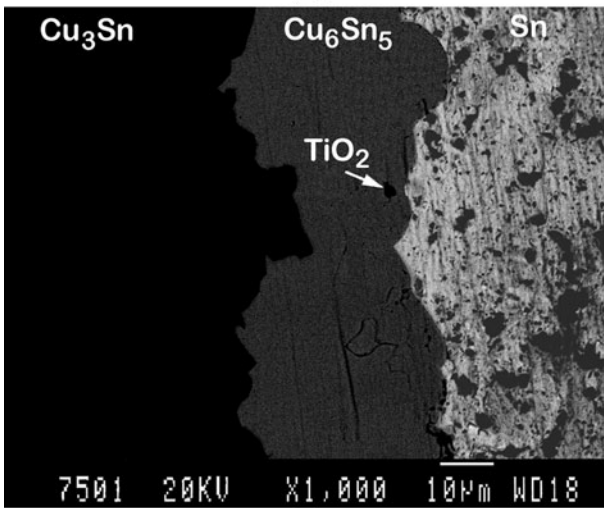
Table I. Summary of Diffusion Data (SI Units)

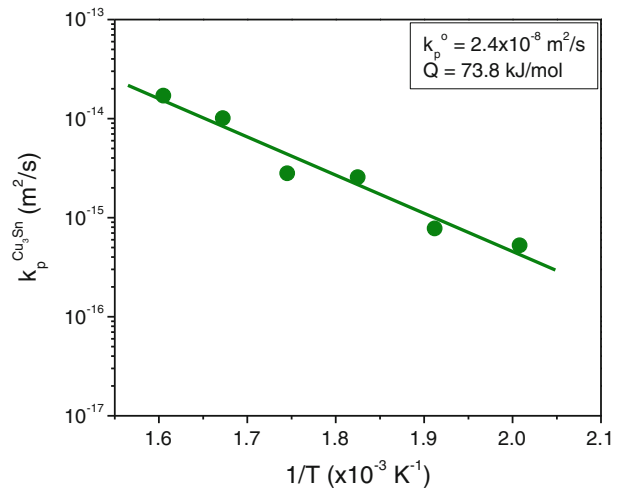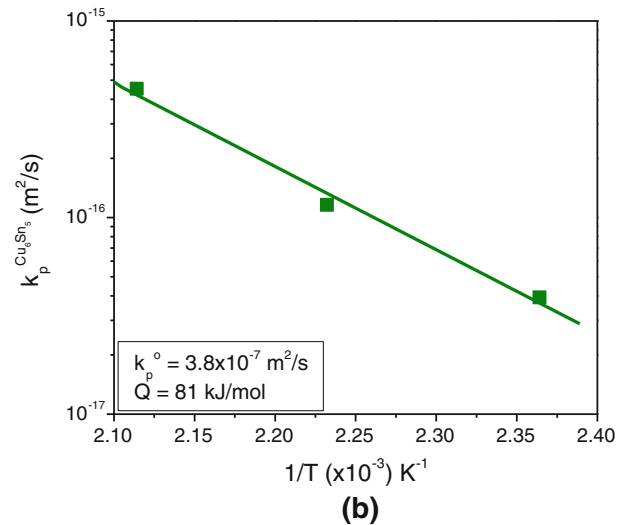| T K (°C)	Cu₃Sn					Cu₆Sn₅				
	$\tilde{D}_{int}^{Cu_3Sn} \times 10^{-16}$	$\frac{D_{Cu}^*}{D_{Sn}^*}$	$\Delta_r G_{Sn}^0$	$D_{Cu}^* \times 10^{-16}$	$D_{Sn}^* \times 10^{-17}$	$\tilde{D}_{int}^{Cu_6Sn_5} \times 10^{-17}$	$\frac{D_{Cu}^*}{D_{Sn}^*}$	$\Delta_r G_{Sn}^0$	$D_{Cu}^* \times 10^{-17}$	$D_{Sn}^* \times 10^{-17}$
423 (150)						0.58	0.42	3370	0.76	1.81
448 (175)						1.72	0.31	3390	1.88	6.06
473 (200)						6.72	0.37	3440	8.77	23.68
498 (225)	0.59	23	29,200	1.19	0.51					
523 (250)	0.87	42	29,200	1.94	0.47					
548 (275)	2.88	29	29,100	6.55	2.25					
573 (300)	3.16	26	28,900	7.45	2.92					
598 (325)	11.3	23	28,800	27.6	12.3					
623 (350)	19.1	31	28,700	50.5	16					

Fig. 2—Incremental diffusion couples show the growth of (a) Cu₃Sn phase annealed at 498 K (225 °C). (b) Polarized micrograph of the interdiffusion zone for a sample annealed at 623 K (350 °C). Enlarged section shows the duplex morphology in the interdiffusion zone separated by the Kirkendall marker plane, as indicated by the white line. (c) Cu₆Sn₅ phase produced at 473 K (200 °C) after 225 h in the interdiffusion zone.

Fig. 3—Parabolic growth of the phases (a) Cu₃Sn and (b) Cu₆Sn₅ measured in the incremental couples is shown.

$$\tilde{D}_{int}^{Cu_3Sn} = \int_{I}^{II} \left\{ \left(N_{Cu}^{Cu_3Sn} D_{Sn}^* + N_{Sn}^{Cu_3Sn} D_{Cu}^* \right) N_{Sn} \right\} d\ln a_{Sn}$$

$$= \left(N_{Cu}^{Cu_3Sn} D_{Sn}^* + N_{Sn}^{Cu_3Sn} D_{Cu}^* \right) N_{Sn}^{Cu_3Sn} \left[\ln a_{Sn}^{II} - \ln a_{Sn}^{I} \right]$$

[10]

where I and II represent the two interfaces from which the product phase can grow. Because the integrated diffusion coefficient considers compounds with very narrow homogeneity ranges, the diffusion parameters and the composition were assumed constant. Further, following the notation in Figure 5(a), and using the standard thermodynamic relation, $\mu_{Sn} = \bar{G}_{Sn}^0 + RT \ln a_{Sn}$, we can write Eq. [10] as

$$\tilde{D}_{int}^{Cu_3Sn} = \left(N_{Cu}^{Cu_3Sn} D_{Sn}^* + N_{Sn}^{Cu_3Sn} D_{Cu}^* \right) \frac{N_{Sn}^{Cu_3Sn} \left(\mu_{Sn}^{II} - \mu_{Sn}^{I} \right)}{RT}$$

$$= -\left(N_{Cu}^{Cu_3Sn} D_{Sn}^* + N_{Sn}^{Cu_3Sn} D_{Cu}^* \right) \frac{N_{Sn}^{Cu_3Sn} \Delta_r G_{Sn}^0}{RT}$$ [11a]

which we will again neglect, as discussed previously. By substituting Eq. [9] into Eq. [1] and using the notation defined in Figure 5(a), we can write
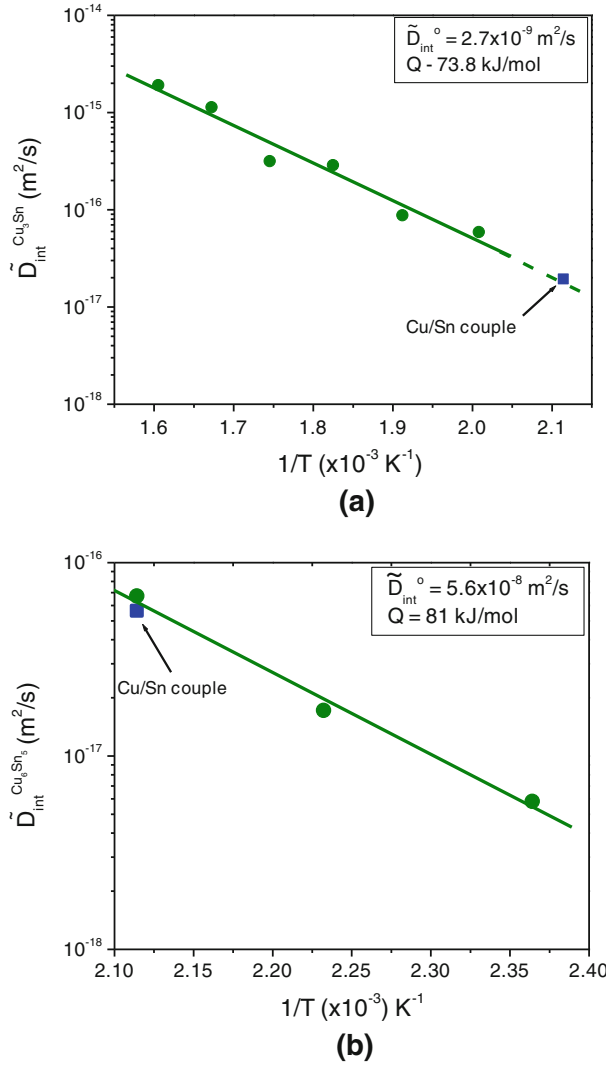
(a)

(b)

Fig. 4—Integrated diffusion coefficients of the phases (*a*) Cu_3Sn and (*b*) Cu_6Sn_5 obtained from the incremental diffusion couples are shown.

(a)

(b)

Fig. 5—Driving forces for the growth of the phases (*a*) Cu_3Sn and (*b*) Cu_6Sn_5 in the incremental diffusion couples are shown.

where G_{Sn}^0 is the free energy of pure Sn, μ_{Sn} is the chemical potential of Sn, $\Delta_r G_{Sn}^0$ is the driving force for the diffusion of Sn in Cu_3Sn phase, as shown in Figure 5(a). It should be noted that $N_{Sn}^{Cu_3Sn} \Delta_r G_{Sn}^0 = N_{Cu}^{Cu_3Sn} \Delta_r G_{Cu}^0$. The driving force for diffusion of elements in the different phases at different temperatures calculated from the data available in the literature[22,23] is also listed in Table I. Similarly, one can develop the relation between the integrated diffusion coefficient of Cu_6Sn_5 phase and the tracer diffusion coefficients using the notation in Figure 5(b) as

$$\tilde{D}_{int}^{Cu_6Sn_5} = -\left(N_{Cu}^{Cu_6Sn_5} D_{Sn}^* + N_{Sn}^{Cu_6Sn_5} D_{Cu}^*\right) \frac{N_{Sn}^{Cu_6Sn_5} \Delta_r G_{Sn}^0}{RT}$$

[11b]

Knowing $\tilde{D}_{int}$, $\Delta_r G_{Sn}^0$, and the ratio D_{Cu}^*/D_{Sn}^* for each phase, the individual tracer coefficients can be

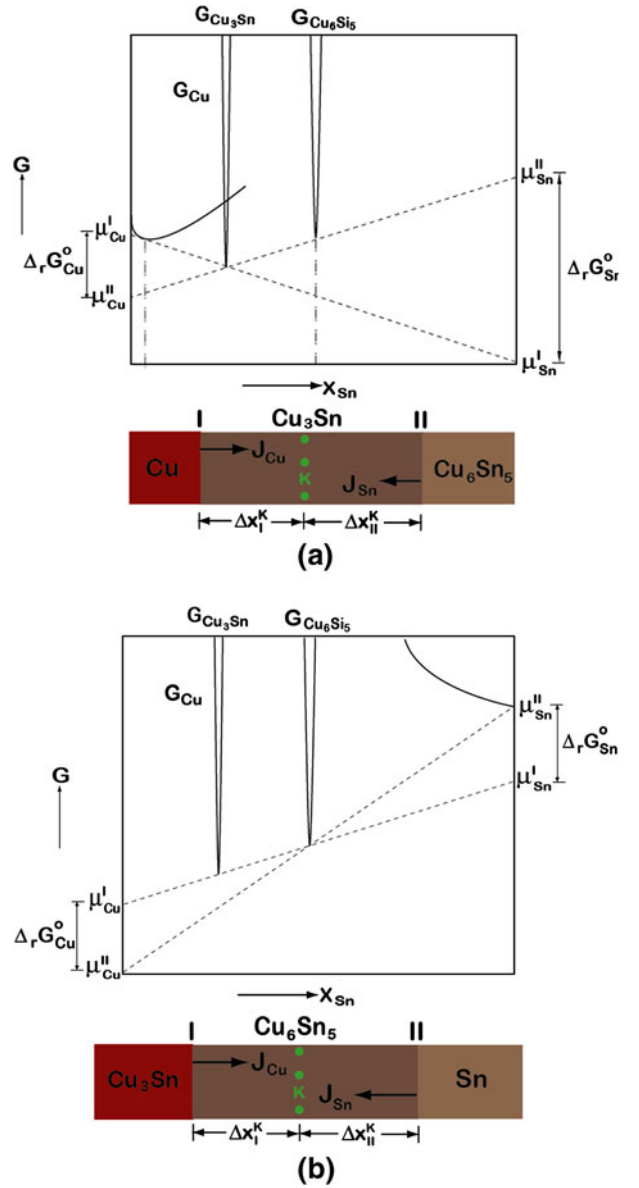calculated, as shown in Figures 6(a) and (b) and as given in Table I. From the slopes for each phase, it is seen that there is not much difference in the activation energies for Sn and Cu tracer diffusivities in each phase.

IV. DISCUSSION

We (a) discuss the possible atomic mechanism of diffusion based on the crystal structure and the data obtained from incremental diffusion couples, (b) use the physicochemical approach[24,25] to understand the interface reactions in the Cu/Sn diffusion couple, and (c) comment on the experimental Cu/Sn diffusion couple results compared to predictions made from data obtained from the incremental couples.
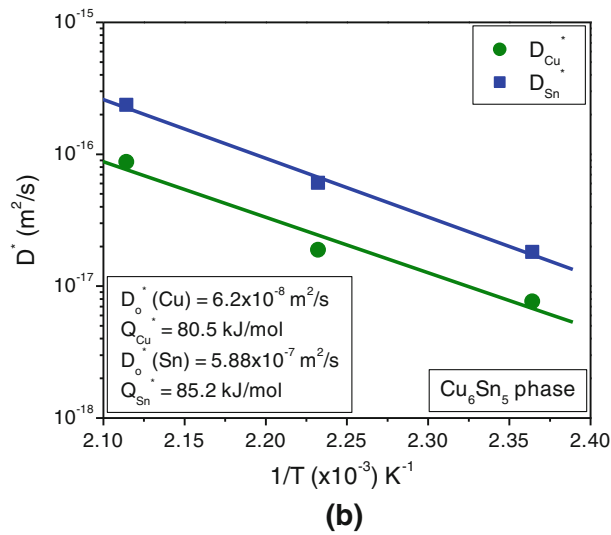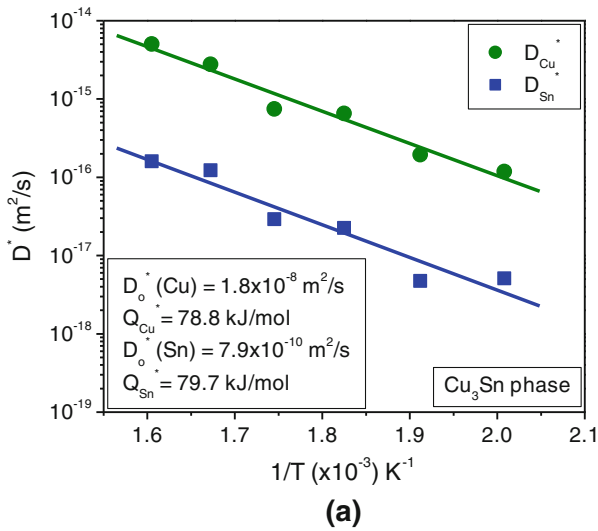
(a)

(b)

Fig. 7—(a) Orthorhombic long period structure of Cu₃Sn (oC80) phase. (b) Cu₃Ti (oP8) structure based on which the crystal structure of Cu₃Sn phase is developed.

(a)

(b)

Fig. 8—(a) Crystal structure of Cu₆Sn₅ phase and (b) the nearest neighbors of atoms.

Fig. 6—Tracer diffusion coefficients of elements Cu and Sn in the phases (a) Cu₃Sn and (b) Cu₆Sn₅ obtained from the incremental diffusion couples are shown.

A. Atomic Mechanisms

1. Cu₃Sn phase

Watanabe et al.[26] found the Cu₃Sn phase to have an orthorhombic long period superstructure with 80 atoms per unit cell (oC80, Cmcm), as shown in Figure 7(a). Each unit of the long period structure has the orthorhombic Cu₃Ti ordered lattice (oP8, DO_a, Pmnm), as shown in Figure 7(b). It is shifted every five units along the b-axis. The Cu₃Ti structure corresponds to an orthorhombically distorted hexagonal close-packed structure. It can be understood that every Cu is surrounded by 8 Cu atoms and 4 Sn atoms, whereas every Sn atom is surrounded by 12 Cu atoms; thus, Cu can diffuse, while in the absence of antistructure defect, Sn cannot. Hence, antisites must be present because the present experiments show that both Sn and Cu are mobile. We note one study of the high-temperature form of the Cu₃Sn composition in the cubic cF16

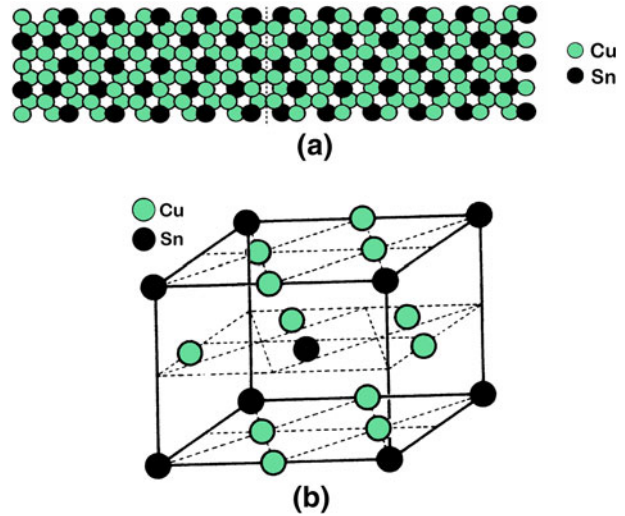(DO_3) structure.[27] However, there is no study available on the defect structure in low-temperature ε-Cu₃Sn phase.

Our measurements may include a contribution from grain boundaries, as indicated by the relatively low value of $Q/RT_m \approx 10$ measured here (taking $T_m = 900$ K [627 °C]). It should be noted that during the growth of the phase, the grain size continuously changes as the layer grows away from the Kirkendall markers, making it difficult to perform a quantitative analysis of the contribution from grain boundary diffusion.

2. Cu_6Sn_5 phase

The Cu_6Sn_5 phase has a partially filled $B8_2$ Ni_2In ($P6_3/mmc$) structure, as shown in Figure 8(a). Older literature[28] indicates that Cu_6Sn_5 has the $B8_1$ NiAs structure. However to achieve proper stoichiometry and match the measured density, partial filling of interstices with Cu is required.[14] Indeed correct density and stoichiometry is achieved with the $B8_2$ structure if the 2a Wyckoff site is occupied by Cu atoms (2 atoms per unit cell), the 2c site is occupied by Sn atoms (2 atoms in a unit cell), and the 2d site is partially filled with Cu (0.4 atom fraction of Cu). If we ignore the extra Cu atoms on the 2d site, we have a $B8_1$ NiAs structure. Then, from Figure 8(b), it must be clear that every Cu atom would be surrounded by 6 Sn atoms and each Sn atom would be surrounded by 6 Cu atoms. However, because of the extra Cu atoms, there will be few Cu-Cu bonds, but still no Sn-Sn bonds. So, if the concentration of structural defects on both sublattices is the same, then because of extra Cu atoms, we might expect that Cu would have a slightly higher diffusion rate. However, in fact, we find experimentally that Sn has a slightly higher diffusion rate than Cu. So, if lattice diffusion is operative, it indicates that the concentration of vacancies on the Sn sublattice and Sn antisite defects must be higher compared to defects on the Cu sites. The low temperature ordering of the $B8_2$ structure[29] may also influence the diffusion processes.

As with Cu_3Sn, the relatively low activation energy of diffusion in Cu_6Sn_5 indicates a contribution from grain boundary diffusion. One might ask whether the higher diffusion rate of Sn compared to Cu in the Cu_6Sn_5 phase is due to the contribution from grain boundaries. For diffusion couples made of Cu-5 pct Ni or Cu-10 pct Ni solid solutions (atomic fraction) with Sn, it was previously noticed that the average grain size of the $(Cu,Ni)_6Sn_5$ decreased by a factor of 10 and the growth rate of the $(Cu,Ni)_6Sn_5$ phase increased by a factor of 8 compared to Cu_6Sn_5 formed in a Cu/Sn couple.[30] This result might be an indication that the diffusion of Sn increases and the diffusion rate of Cu decreases when the contribution from grain boundary diffusion increases. Further investigation on this topic is necessary.

B. Growth Mechanism of Intermetallics in Cu/Sn Couple Using the Physicochemical Approach

In this section, we shall use the diffusion parameters obtained from the incremental diffusion couples to understand the growth mechanism of the phases in the Cu-Sn couple using the physicochemical approach.[24,25] This approach focuses on the events at the three
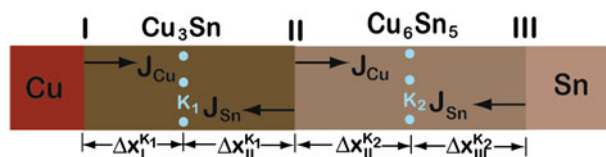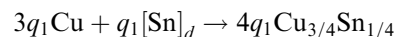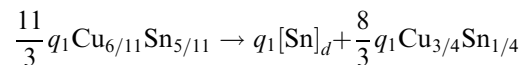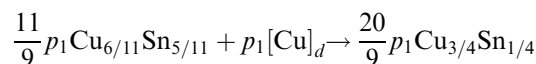

Fig. 9—Diffusion of elements and growth of the phases in Cu-Sn diffusion couple.

interfaces, treating them like chemical reactions. Figure 9 introduces the possible dissociation or reactions of elements and compounds to be analyzed as the intermetallics dissolve or grow. It must be clear that a complicated interdependent diffusion process must be operative at interface II, where the Cu_3Sn phase could grow by consuming the Cu_6Sn_5 phase or get consumed because of the growth of Cu_6Sn_5 phase. To determine the relative contribution of the two, we assume they both occur simultaneously and write the hypothetical reaction/dissociation scheme at the interfaces as follows.
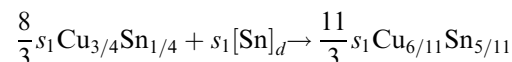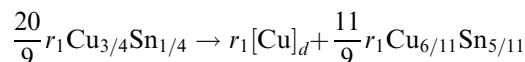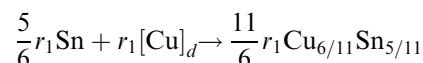
Interface I:

$$3q_1Cu + q_1[Sn]_d \rightarrow 4q_1Cu_{3/4}Sn_{1/4}$$

Interface II—Cu_3Sn side:

$$\frac{11}{9}p_1Cu_{6/11}Sn_{5/11} + p_1[Cu]_d \rightarrow \frac{20}{9}p_1Cu_{3/4}Sn_{1/4}$$

$$\frac{11}{3}q_1Cu_{6/11}Sn_{5/11} \rightarrow q_1[Sn]_d + \frac{8}{3}q_1Cu_{3/4}Sn_{1/4}$$

Interface II—Cu_6Sn_5 side:

$$\frac{20}{9}r_1Cu_{3/4}Sn_{1/4} \rightarrow r_1[Cu]_d + \frac{11}{9}r_1Cu_{6/11}Sn_{5/11}$$

$$\frac{8}{3}s_1Cu_{3/4}Sn_{1/4} + s_1[Sn]_d \rightarrow \frac{11}{3}s_1Cu_{6/11}Sn_{5/11}$$

Interface III:

$$\frac{5}{6}r_1Sn + r_1[Cu]_d \rightarrow \frac{11}{6}r_1Cu_{6/11}Sn_{5/11}$$

Here, p_1 and q_1 are the moles of Cu and Sn, respectively, transferred per unit area through the Cu_3Sn phase during total diffusion time, t. Similarly, r_1 and s_1 are the number of moles of Cu and Sn transported during interaction per unit area through the Cu_6Sn_5-phase layer. From the equations written previously, it must be clear that at interface II, $\left(\frac{20}{9}p_1 + \frac{8}{3}q_1\right)$ moles of Cu_3Sn grow, but $\left(\frac{20}{9}r_1 + \frac{8}{3}s_1\right)$ moles get consumed because of the growth of Cu_6Sn_5 phase. Similarly, $\left(\frac{11}{9}r_1 + \frac{11}{3}s_1\right)$ moles of Cu_6Sn_5 grow at the same interface, but $\left(\frac{11}{9}p_1 + \frac{11}{3}q_1\right)$ moles get consumed by Cu_3Sn phase. Let us consider, as shown in Figure 9, that a Kirkendall marker plane originating from the original

Cu/Sn interface is present in both phases after diffusion. We then write

$$4q_1 \times V_m^{Cu_3Sn} = \Delta x_I^{K_1}$$

$$\left(\frac{20}{9}p_1 + \frac{8}{3}q_1 - \frac{20}{9}r_1 - \frac{8}{3}s_1\right) \times V_m^{Cu_3Sn} = \Delta x_{II}^{K_1}$$

$$\left(\frac{11}{9}r_1 + \frac{11}{3}s_1 - \frac{11}{9}p_1 - \frac{11}{3}q_1\right) \times V_m^{Cu_6Sn_5} = \Delta x_{II}^{K_2} \quad [12]$$

$$\frac{11}{6}r_1 \times V_m^{Cu_6Sn_5} = \Delta x_{III}^{K_2}$$

where $\Delta x_I^{K_1}$ and $\Delta x_{II}^{K_1}$ are the thickness of the sublayers in the Cu_3Sn phase. $\Delta x_{II}^{K_2}$ and $\Delta x_{III}^{K_2}$ are the thickness of sublayers in the Cu_6Sn_5 phase. Because of the Boltzmann solution of Fick's second law, the integrated diffusion coefficient of the phases and the ratio of tracer diffusion coefficient of the species in these phases can be written as

$$\tilde{D}_{int}^{Cu_3Sn} = \frac{V_m^{Cu_3Sn}}{2t}\left[N_{Cu}^{Cu_3Sn}q_1 + N_{Sn}^{Cu_3Sn}p_1\right]\Delta x^{Cu_3Sn}$$

$$= \frac{V_m^{Cu_3Sn}}{2t}\left[N_{Cu}^{Cu_3Sn}q_1 + N_{Sn}^{Cu_3Sn}p_1\right]\left(\Delta x_I^{K_1} + \Delta x_{II}^{K_1}\right)$$

$$[13a]$$

$$\tilde{D}_{int}^{Cu_6Sn_5} = \frac{V_m^{Cu_6Sn_5}}{2t}\left[N_{Cu}^{Cu_6Sn_5}s_1 + N_{Sn}^{Cu_6Sn_5}r_1\right]\Delta x^{Cu_6Sn_5}$$

$$= \frac{V_m^{Cu_6Sn_5}}{2t}\left[N_{Cu}^{Cu_6Sn_5}s_1 + N_{Sn}^{Cu_6Sn_5}r_1\right]\left(\Delta x_{II}^{K_2} + \Delta x_{III}^{K_2}\right)$$

$$[13b]$$

$$\left.\frac{D_{Cu}^*}{D_{Sn}^*}\right|_{Cu_3Sn} = \frac{p_1}{q_1} \quad [13c]$$

$$\left.\frac{D_{Cu}^*}{D_{Sn}^*}\right|_{Cu_6Sn_5} = \frac{r_1}{s_1} \quad [13d]$$

Now our target is to predict the layer thickness of the phases and the position of the marker plane position in the Cu/Sn diffusion couple at 473 K (200 °C) and 225 hours from the knowledge of the diffusion parameters obtained from the incremental diffusion couple technique. The integrated diffusion coefficient of the phases and the ratio of diffusivities are materials constant and do not depend on the end member compositions. It should be noted that the total thickness of the phase layers only depends on the integrated diffusion coefficients. Indeed this is the utility of Wagner's definition of the integrated diffusion coefficients. On the other hand, the thickness of the sublayers, that is, the position of the marker plane(s), depends on the relative mobilities of species. The data used in the calculations for 473 K (200 °C) are $\tilde{D}_{int}^{Cu_3Sn} = 1.85 \times 10^{-17}\,m^2/s$, $\tilde{D}_{int}^{Cu_6Sn_5} = 6.72 \times 10^{-17}\,m^2/s$, $D_{Cu}^*|_{Cu_3Sn} = 3.53 \times 10^{-17}\,m^2/s$, $D_{Sn}^*|_{Cu_3Sn} = 1.21 \times 10^{-18}\,m^2/s$, $D_{Cu}^*|_{Cu_6Sn_5} = 8.77 \times 10^{-17}\,m^2/s$, and $D_{Sn}^*|_{Cu_6Sn_5} = 2.37 \times 10^{-16}\,m^2/s$. For Cu_3Sn phase at 473 K (200 °C), we

used the extrapolation from higher temperatures. After solving Eq. [13], we determine the flux parameters as $p_1 = 1.52\,mol/m^2$, $q_1 = 0.0515\,mol/m^2$, $r_1 = 0.291\,mol/m^2$, and $s_1 = 0.788\,mol/m^2$. The sublayer thicknesses are calculated as $\Delta x_I^{K_1} = 1.77\,\mu m$, $\Delta x_{II}^{K_1} = 6.58\,\mu m$, $\Delta x_{II}^{K_2} = 12.68\,\mu m$, and $\Delta x_{III}^{K_2} = 5.64\,\mu m$. The total calculated layer thickness of the phases $\Delta x^{Cu_3Sn} = \Delta x_I^{K_1} + \Delta x_{II}^{K_1} = 8.35\,\mu m$ and $\Delta x^{Cu_6Sn_5}\left(= \Delta x_{II}^{K_2} + \Delta x_{II}^{K_2}\right) = 18.32\,\mu m$.

C. Comparison to Cu/Sn Experimental Results

We find reasonable agreement between the thicknesses of the phase layers calculated using the physicochemical approach with data obtained from the incremental couples and the thicknesses measured experimentally in the Cu/Sn diffusion couple at 473 K (200 °C) and 225 hours; viz. 9 and 16.4 μm for Cu_3Sn and Cu_6Sn_5, respectively. This success is not unexpected because the diffusion parameters are materials constants for phases and should be the same irrespective of end member compositions in a diffusion couple. Regarding the marker locations, the calculated thicknesses of the sublayers are all positive, indicating that both phase layers should have Kirkendall marker planes. However, it can be seen in the Cu/Sn diffusion couple that we have found a marker plane only in the Cu_6Sn_5 phase. In Cu_6Sn_5, we predict a location of markers $\Delta x_{II}^{K_2} = 12.68\,\mu m$ compared to the 7 μm measured. This difference and the absence of the second Kirkendall plane lead us to suspect that the detailed growth mechanism of each intermetallic in the Cu/Sn diffusion couple is affected by the other intermetallic to some degree. In particular, we discuss two issues: the presence of nonplanar interfaces between phases and the absence of double Kirkendall planes in the Cu/Sn couple experiment. We shall discuss these issues in turn.

It is clear that Cu_3Sn grows with almost uniform thickness in the Cu/Cu_6Sn_5 incremental couple. Little or no diffusion through Cu_6Sn_5 is required in this incremental couple as the Cu_6Sn_5 phase merely dissolves. On the other hand, for both the Cu/Sn and Cu_3Sn/Sn couples, diffusion through the Cu_6Sn_5 phase is necessary, as indicated from the location of the Kirkendall markers within the Cu_6Sn_5 phase. It must form at both interfaces. We surmise that the Cu_6Sn_5 phase layer, as shown in Figures 1 and 2(c), is highly nonuniform in thickness because of the low temperature ordering of the crystal structure of Cu_6Sn_5,[29] in which the diffusion rate is expected to be highly anisotropic. The presence of grain boundaries within the intermetallic layer and the necessity for grain boundary grooves at the interface with the other phases can also contribute to the wavy nature of the interfaces. Further research on this waviness is warranted.

As to the subject of the absence of double Kirkendall planes in the Cu/Sn couple, we perform the following analysis. The velocity of the markers is dependent on the difference in intrinsic diffusivities of the species and

can be determined in the two different phases as follows:[31]

$$V_m^{Cu_3Sn}(q_1 - p_1) = 2tv_{K_1}^{Cu_3Sn} = x_{K_1}^{Cu_3Sn} - x_0 \qquad [14a]$$

$$V_m^{Cu_6Sn_5}(s_1 - r_1) = 2tv_{K_2}^{Cu_6Sn_5} = x_{K_2}^{Cu_6Sn_5} - x_0 \qquad [14b]$$

Further, in a diffusion-controlled interaction, the inert markers positioned at the location of the original interface between the reactants ("Kirkendall plane") are the only markers that stay at a position of constant composition during the entire diffusion anneal and move parabolically in time with a velocity:

$$v_K = \frac{dx}{dt} = \frac{x_K - x_0}{2t} = \frac{x_K}{2t} \qquad [15]$$

where x_K and x_0 $(=0)$ are the positions of the Kirkendall plane at times $t = t$ and $t = 0$, respectively.

The position(s) and the number of the Kirkendall plane(s) can be found from the points of intersection between the velocity curve vs distance curve plotted as $2tv$ vs x (calculated by Eqs. [14a] and [b]) and the straight line $2tv_K = x_K$ (determined by Eq. [15]). We consider the values of $p_1 = 1.52 \text{ mol/m}^2$, $q_1 = 0.0515 \text{ mol/m}^2$, $r_1 = 0.291 \text{ mol/m}^2$, and $s_1 = 0.788 \text{ mol/m}^2$, as already calculated in the previous section, to find the values from Eq. [14] and plot the velocity diagram, as shown in Figure 10. It can be seen that the straight line $2tv_K = x_K$ intersects the $2tv$ vs x plot twice at locations labeled K_1 and K_2. The intersecting points indicate the position where marker planes should occur.[25] So, the question here is why we do not find any markers in the Cu_3Sn phase in the experimental results, although calculation shows that markers should be present in this phase along with the marker in the Cu_6Sn_5 phase. One might think that the diffusion behaviors in incremental couples and the Cu/Sn

diffusion couple are different. It should be noted that, theoretically, the diffusion parameters are materials constant and do not depend on the end member composition. This is also validated from the fact that the average thicknesses of the phases calculated in the Cu/Sn diffusion couple using the data determined from the incremental diffusion couple are found to agree within the limit of experimental errors. Because of the known thickness of the layers and their molar volumes, the position of the initial contact plane x_0 is known. Further, the absence or presence of the marker plane in the Cu_3Sn phase also should be determined because of the presence of the marker plane in the Cu_6Sn_5 phase. The position of the x_0 and $x_{K_2}^{Cu_6Sn_5}$ planes will fix the slope of the straight line $2tv_K = x_K$. If this line hits the velocity curve $2tv$ vs x in the Cu_3Sn phase region, which is the case here, the Kirkendall marker plane also should be present in this phase.

One possible reason why we do not find any markers in the Cu_3Sn would be a change in the relative mobility of species at 473 K (200 °C) compared to higher temperatures so that the line $2tv_K = x_K$ misses the velocity curve of the Cu_3Sn phase such that $\Delta x_{II}^{K_1} \leq 0$. A negative prediction means that no Kirkendall plane would be present. We can compute the value that $2tv_{K_1}^{Cu_3Sn}$ would have to be in order for $\Delta x_{II}^{K_1} = 0$, as shown in Figure 10, and obtain $2tv_{K_1}^{Cu_3Sn} = -6.53 \text{ m/s}$. From the knowledge of $\tilde{D}_{int}^{Cu_3Sn} = 1.85 \times 10^{-17} \text{ m}^2/\text{s}$, we solve Eqs. [13a] and [14a] to find the values of fluxes as $p_1 = 0.988$ and $q_1 = 0.228 \text{ mol/m}^2$ for this marginal case and $\left.\frac{D_{Cu}^*}{D_{Sn}^*}\right|_{Cu_3Sn} = \frac{p_1}{q_1} \leq 4.33$. Although we could not measure the relative mobilities of the species at 473 K (200 °C), the data extended from 498 K to 625 K (225 °C to 350 °C) indicate that the ratio at this temperature remains around ~30 (Table I). It is unlikely the ratio would change to 4.33 at 473 K (200 °C).

A second reason for not finding any marker plane in the Cu_3Sn phase might be a large incubation (nucleation) time for the Cu_3Sn compared to the Cu_6Sn_5 phase. If one phase has a larger incubation time than the other because of a nucleation problem, then all the markers will be trapped in the first phase to form. Markers should be present in both phases experimentally as long as both phases have nucleated before the thickness of one intermetallic exceeds the marker size. It is very difficult to determine the incubation period of the phases by extrapolating the results back to zero time because of the uncertainty inherent in the thickness measurements due to the waviness of the phase boundaries.

There are several ideas developed to predict the sequence of formation of phases in a diffusion couple.[32–35] An excellent review is published by Reference 36. However no single theory appears to predict the sequence observed in all the systems. Determination of the first phase formation is possible, only when complete knowledge on driving force and interface energy are available for all the phases in the interdiffusion zone to predict the nucleation process. Although the data on driving force can be determined experimentally, the data on interface energy are not available.
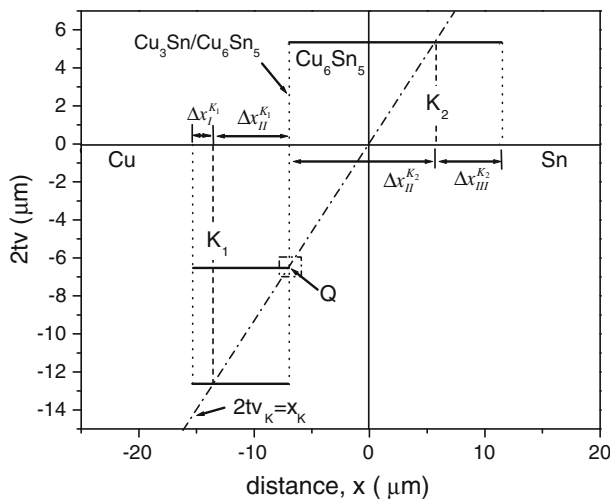

Fig. 10—Velocity diagram is shown for the Cu/Sn diffusion couple. The straight line $2tv_K = x_K$ intersects the $2tv$ vs x line twice at locations K_1 and K_2, indicating the bifurcation of the marker plane into two locations.
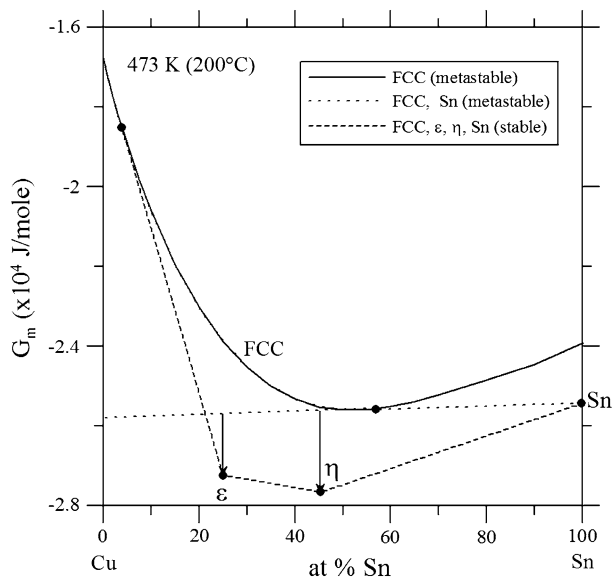
Fig. 11—Cu-Sn molar free energy *vs* at. pct Sn at 473 K (200 °C) showing the thermodynamic driving force (arrows) for nucleation of Cu_3Sn and Cu_6Sn_5 at a Cu/Sn interface in a diffusion couple.

It is, nonetheless, interesting to examine the thermodynamic driving force for nucleation of the two intermetallics on the Cu/Sn solid interface in a manner similar to that described by Philibert,[37] used by Lee *et al.*,[35] and validated by Vianco and Frear[38] for Cu in contact with liquid solders. For the present solid-state case, the thermodynamic assessment of Reference 22 was used. Figure 11 shows the metastable interfacial equilibrium common tangent that must exist just prior to the nucleation of Cu_3Sn and Cu_6Sn_5. The driving force for nucleation of either intermetallic is the horizontal difference between the tangent line and the intermetallic of interest. A slightly larger driving force exists for Cu_6Sn_5 than for Cu_3Sn, so Cu_6Sn_5 might form first. Of course, knowledge of surface energies or nucleating sites would be required to fully support this hypothesis. It is also known that Cu_3Sn often does not form at room temperature,[9,38] indicating that a significant nucleation barrier must exist for Cu_3Sn.

V. CONCLUSIONS

1. Because of the narrow and difficult to measure composition range of the Cu-Sn intermetallics, the method of Wagner was used to determine the integrated interdiffusion coefficients for Cu_3Sn and Cu_6Sn_5 from incremental diffusion couples Cu/Cu_6Sn_5 and Cu_3Sn/Sn in the respective ranges 498 K to 623 K and 393 K to 473 K (225 °C to 350 °C and 150 °C to 200 °C). The relatively low activation energies for diffusion compared to that expected for materials with the melting points of the intermetallics suggests a significant contribution from grain boundary diffusion.
2. Using marker measurements and the analysis method proposed by van Loo, the ratios of tracer diffusivities have been determined for the intermetallics in the same temperature ranges; *viz.*, for Cu_3Sn, $D^*_{Cu}/D^*_{Sn} \approx 30$; and for Cu_6Sn_5, $D^*_{Cu}/D^*_{Sn} \approx 0.35$. In addition to the ratios, the individual values of the tracer diffusivities are reported and are found to have similar activation energies.
3. When data from the incremental diffusion couples are applied to predict the behavior of a Cu/Sn diffusion couple, the individual Cu_3Sn and Cu_6Sn_5 layer thicknesses agree with the experiment.
4. Data from the incremental diffusion couples predict a bifurcation of Kirkendall markers for the Cu/Sn diffusion couple into both intermetallic phases. However, this is not observed experimentally. Possible reasons for the absence of two Kirkendall planes are given.
5. The extremely high rate of diffusion of Cu in the Sn phase determined previously by Reference 6 is not present in the intermetallic phases. This fact should be considered when one analyzes the location of Kirkendall porosity, if present, in Cu/Sn diffusion problems.

NOTE ADDED IN PROOF

The recent research[39] conducted at Purdue University reports qualitatively similar results to this article.

REFERENCES

1. D.R. Frear and P.T. Vianco: *Metall. Mater. Trans. A*, 1994, vol. 25A, pp. 1509–23.
2. Z. Mei, A.J. Sunwoo, and J.W. Morris: *Metall. Trans. A*, 1992, vol. 23A, pp. 857–64.
3. D.B. Butrymowicz: *Diffusion Rate Data and Mass Transport Phenomena for Copper Systems—Part II*, INCRA Monograph Series V (International Copper Research Association), Diffusion in Metals Data Center, National Bureau of Standards, Washington, DC, 1981, pp. 398–475.
4. L.C.C. da Silva and R.F. Mehl: *Trans. AIME*, 1951, vol. 191, pp. 155–73.
5. H. Oikawa and A. Hosoi: *Scripta Metall.*, 1975, vol. 9, pp. 823–28.
6. B.F. Dyson, T.R. Anthony, and D. Turnbull: *J. Appl. Phys.*, 1967, vol. 38, p. 3408.
7. M. Onishi and H. Fujibuchi: *Trans. Jpn. Inst. Met.*, 1975, vol. 16, pp. 539–47.
8. C. Wagner: *Acta Metall.*, 1969, vol. 17, pp. 99–107.
9. K.N. Tu and R.D. Thompson: *Acta Metall.*, 1982, vol. 30, pp. 947–52.
10. A. Paul, A.A. Kodentsov, and F.J.J. van Loo: *Z. Metallkd.*, 2004, vol. 95, pp. 913–20.

11. R.J. Schaeffer, F.S. Biancaniello, and R.D. Jiggetts: in *The Metal Science of Joining*, M.J. Cieslak, J.H. Perpezko, S. Kang, and M.E. Glicksman, eds., TMS-AIME, Warrendale, PA, 1992, pp. 175–81.
12. E. Chason, N. Jadhav, W.L. Chan, L. Reinbold, and K.S. Kumar: *Appl. Phys. Lett.,* 2008, vol. 92, art. no. 171901.
13. K.S. Kumar, L. Reinbold, A.F. Bower, and E. Chason: *J. Mater. Res.*, 2008, vol. 23, pp. 2916–34.
14. R.J. Fields, S.R. Low, and G.K. Lucey: in *The Metal Science of Joining*, M.J. Cieslak, J.H. Perepezko, S. Kang, and M.E. Glicksman, eds., TMS-AIME, Warrendale, PA, 1992, pp. 165–73.
15. W.J. Boettinger, C.A. Handwerker, and L.C. Smith: in *The Metal Science of Joining*, M.J. Cieslak, J.H. Perepezko, S. Kang, and M.E. Glicksman, eds., TMS-AIME, Warrendale, PA, 1992, pp. 183–89.
16. P. Villars and L.D. Calvert: *Pearson's Handbook of Crystallographic Data for Intermetallic Phases*, ASM, Metals Park OH, 1985, p. 2030.
17. F.J.J. van Loo: *Acta Metall.*, 1970, vol. 18, pp. 1107–11.
18. F. Sauer and V. Freise: *Z. Electrochem.*, 1962, vol. 66, pp. 353–63.
19. J.R. Manning: *Acta Metall.*, 1967, vol. 15, pp. 817–26.
20. I.V. Belova and G.E. Murch: *Def. Diffus. Forum*, 2003, vols. 213–215 (2), pp. 95–106.
21. A. Paul, A.A. Kodentsov, and F.J.J. van Loo: *J. Alloys Compds.*, 2005, vol. 403, pp. 147–53.
22. J.H. Shim, C.S. Oh, B.J. Lee, and D.N. Lee: *Z. Metallkd.*, 1996, vol. 87, pp. 205–12.
23. X.J. Liu, H.S. Liu, I. Ohnuma, R. Kainuma, K. Ishida, S. Itabashi, K. Kameda, and K. Yamaguchi: *J. Electron Mater.*, 2001, vol. 30, pp. 1093–03.
24. F.J.J. van Loo, B. Pieraggi, and R.A. Rapp: *Acta Metall. Mater.*, 1990, vol. 38, pp. 1769–79.
25. A. Paul, M.J.H. van Dal, A.A. Kodentsov, and F.J.J. van Loo: *Acta Mater.*, 2004, vol. 52, pp. 623–30.
26. Y. Watanabe, Y. Fujinaga, and H. Iwasaki: *Acta Cryst. B*, 1983, vol. 39, pp. 306–11.
27. I.V. Belova and G.E. Murch: *J. Phys. Chem. Solids*, 1998, vol. 59, pp. 1–6.
28. A. Gangulee, G.C. Das, and M.B. Bever: *Metall. Trans.*, 1973, vol. 4, pp. 2063–66.
29. A.-K. Larsson, L. Stenberg, and S. Lidin: *Acta Cryst.*, 1994, vol. B50, pp. 636–43.
30. A. Paul: Ph.D. Thesis, Eindhoven University of Technology, Eindhoven, 2004.
31. C. Ghosh and A. Paul: *Acta Mater.*, 2007, vol. 55, pp. 1927–39.
32. K.N. Tu, G. Ottaviani, U. Gösele, and H. Föll: *J. Appl. Phys.*, 1983, vol. 54, pp. 758–63.
33. R. Pretorius, A.M. Vredenberg, and F.W. Saris: *Mater. Lett.*, 1990, vol. 9, pp. 494–99.
34. R. Pretorius, A.M. Vredenberg, F.W. Saris, and R. De Reus: *J. Appl. Phys.*, 1991, vol. 70, pp. 3636–46.
35. B.J. Lee, N.M. Hwang, and H.M. Lee: *Acta Mater.*, 1997, vol. 45, pp. 1867–74.
36. V.I. Dybkov: *Powder Metall. Met. Ceram.*, 1996, vol. 35, pp. 355–59.
37. J. Philibert: *Atom Movements—Diffusion and Mass Transport in Solids*, Les Editions de Physique, 1991, p. 423.
38. P.T. Vianco and D.R. Frear: *J. Met.*, 1993, vol. 45, pp. 14–19.
39. S. Kumar, C.A Handwerker, and M. Dayananda: Paper presented at the 2009 MS&T Meeting, Pittsburgh, PA, Oct. 2009.